Bistability and chaos at low levels of quanta

T. V. Gevorgyan,[1,*] A. R. Shahinyan,[1,2,†] Lock Yue Chew,[3,‡] and G. Yu. Kryuchkyan[1,2,§]
[1]*Institute for Physical Research, National Academy of Sciences, Ashtarak-2, 0203 Ashtarak, Armenia*
[2]*Yerevan State University, Alex Manoogian 1, 0025 Yerevan, Armenia*
[3]*Nanyang Technological University, 21 Nanyang Link, SPMS-PAP-04-04, Singapore 637371*
(Received 8 February 2013; revised manuscript received 9 June 2013; published 12 August 2013)

We study nonlinear phenomena of bistability and chaos at a level of few quanta. For this purpose, we consider a single-mode dissipative oscillator with strong Kerr nonlinearity with respect to the dissipation rate driven by a monochromatic force as well as by a train of Gaussian pulses. The quantum effects and decoherence in the oscillatory mode are investigated in the framework of the purity of states and the Wigner functions calculated from the master equation. We demonstrate the quantum chaotic regime by means of a comparison between the contour plots of the Wigner functions and the strange attractors on the classical Poincaré section. Considering bistability at a low limit of quanta, we analyze the minimal level of excitation numbers at which the bistable regime of the system is displayed. We also discuss the formation of an oscillatory chaotic regime by varying oscillatory excitation numbers at ranges of a few quanta. We demonstrate quantum-interference phenomena that are assisted hysteresis-cycle behavior and quantum chaos for the oscillator driven by a train of Gaussian pulses. We establish the border of quantum-classical correspondence for chaotic regimes in the case of strong nonlinearities.

DOI: 10.1103/PhysRevE.88.022910 PACS number(s): 05.45.Mt, 42.65.Pc, 42.50.Dv

I. INTRODUCTION

Nonlinear dissipative oscillators (NDO) operating in the quantum regime are of particular significance to fundamental and applied sciences because they are pertinent to the engineering of nonclassical states in basic quantum optical systems and the realization of quantum logic. An important implementation of NDO has been achieved recently in the context of superconducting devices based on the nonlinearity of the Josephson junction (JJ), which is known to exhibit a wide variety of quantum phenomena (see Refs. [1–9]). In fact, the dynamics in some of these devices is analogous to those of a quantum particle residing in an oscillatory anharmonic potential [10]. Furthermore, a single nonlinear oscillator and systems of nonlinear oscillators are basic theoretical models of various nanoelectromechanical and nano-optomechanical devices. Exciting technological advances in the fabrication and control of such devices [11–14] have become possible in the last decade, leading to an increase in interest on the exploitation of the remarkable combination of properties of these devices, such as small mass, high operating frequency, large quality factor, and easily accessible nonlinearity, to a broad variety of research areas and applications. In many cases, nanomechanical oscillators are fundamental to the development of a host of nanotechnological applications. They are ideal candidates for the probing of the quantum limits of mechanical motion within an experimental setting. Moreover, they are the basis of various precision measurements [15–17]. They are also useful for basic research in the mesoscopic physics of phonons [18] and the general study of the behavior of mechanical degrees of freedom at the interface between the quantum and the classical worlds [19].

The efficiency of quantum oscillatory effects requires a high nonlinearity with respect to dissipation. However, for weak damping, even a small nonlinearity can become important. The successful development of driven NDO in the quantum regime requires the system to be cooled to the ground state. Indeed, significant advances have been made that achieve this by attaining a temperature far below the environment [20–26].

It is well known that the bistability of the classically driven NDO [27] results from the induced dependency of the oscillatory frequency or the amplitude on the underlying nonlinearity. The corresponding systems describe amplifiers which are ubiquitous in experimental physics. In particular, a bistable amplifier based on the Josephson junction has been discussed in [28]. In [29,30], the dynamical bifurcation of a rf-biased Josephson junction was proposed as a basis for the amplification of quantum signals. Although the bistability has often been treated as a classical signature of the NDO, the quantum dynamics in the bistable region is a new subject that has been pursued in recent years [31–34].

The quantum dynamics of an oscillator is naturally described by the Fock states, which have a definite number of energy quanta. However, these states are hard to create in experiments because the excitation number of oscillatory systems usually leads to the production of coherent states instead of quantum Fock states. Nevertheless, quantum oscillatory states can be prepared and can be manipulated by coupling the oscillators to atomic systems driven by classical pulses. The systematic procedure has been proposed in Ref. [35] and has been demonstrated for the deterministic preparation of mechanical oscillatory Fock states with trapped ions [36], in cavity QEDs with Rydberg atoms [37], and in a solid-state circuit QED for the deterministic preparation of photon number states in a resonator by interposing a highly nonlinear Josephson phase qubit between a superconducting resonator [38].

Because of the nonlinearity within NDO, transition frequencies between energy levels are different in the quantum regime. For example, it is known that strong nonlinearity can

*t_gevorgyan@ysu.am
†anna_shahinyan@ysu.am
‡lockyue@ntu.edu.sg
§kryuchkyan@ysu.am

enable spectroscopic identification and selective excitation of transitions between Fock states. In consequence, it is possible to prepare the NDO at low levels of quanta in this regime. Furthermore, it has been shown in this approach that the production of Fock states, as well as the superposition of Fock states or qubits, can also be realized in the overtransient regime of an anharmonic dissipative oscillator without any interactions with atomic and spin-1/2 systems and with complete consideration of decoherence effects [39]. To meet this goal, strong Kerr nonlinearity as well as the excitation of resolved lower oscillatory energy levels with a specific train of Gaussian pulses have been considered.

In this paper, we consider NDO in the regime of low levels of excitation to investigate the problems of quantum bistability and chaos. Our goal of the paper is twofold. First, we consider bistability on a few oscillatory excitation numbers for a NDO driven by monochromatic force. Note that bistability on a few excitation numbers is attractive for ultralow power operation. Nonetheless, it has practical problems related to quantum fluctuation-induced spontaneous switching. For this part, we shall demonstrate the production of quantum interference between bistable branches for a NDO driven by a train of Gaussian pulses. It should be mentioned that bistability on few photon regimes has already been investigated theoretically [40,41] as well as experimentally [42] in the area of single-atom cavity quantum electrodynamics.

The other part of the paper is devoted to the investigation of quantum chaos in the oscillator low level excitation regime of the pulsed NDO. Much research on the subject of classical and quantum chaos has been done on the basis of the kicked rotor, which exhibits regions of regular and chaotic motion. The experimental realization and observation of the model with the consideration of dissipation and decoherence effects have been carried out on a gas of ultracold atoms in a magneto-optical trap subjected to a pulsed standing wave [43,44]. In another context, a parametrically kicked nonlinear oscillator model was proposed to be realized in a cavity involving Kerr nonlinearity in Ref. [45]. It had been shown that a more promising realization of this system, including the quantum regime, can be achieved via the dynamics of cooled and trapped ions, interacting with a periodic sequence of both standing wave pulses and Gaussian laser pulses [46]. Recently, the quantum chaotic behavior of the quantum kicked top model of a single atom has been experimentally realized [47]. The transition to classical chaos for a system with coupled internal (spin) and external (motional) degrees of freedom has also been considered [48]. The other important goal (see also [49,50]) of the paper is on quantum dissipative chaos of a NDO driven by a train of Gaussian pulses at low levels of quanta and in complete consideration of dissipation and decoherence. In this way, quantum dissipative chaos at the limit of low levels of excitation numbers is considered in this paper.

The analysis is performed within the framework of a master equation and the method of quantum trajectories based on oscillatory excitation numbers, the Wigner function, and the purity of quantum states. As a result, our original results on bistability and chaos obtained from the quantum treatment are well grounded. Nevertheless, for completeness, we have also compared some of these results with the analogous ones determined from the semiclassical equation.

The paper is organized as follows. In Sec. II, we give a short description of the pulsed NDO. In Sec. III, we investigate bistability at the level of a few quanta for a NDO driven by monochromatic force. In Sec. IV, we consider the production of quantum interference at the bistable regime of the NDO driven by a train of Gaussian pulses. In Sec. V, we study quantum dissipative chaos at the limit of low levels of excitation numbers for a NDO driven by a train of Gaussian pulses. Finally, we summarize our results in Sec. VI.

II. THE MODEL: SHORT DESCRIPTION

The Hamiltonian of an anharmonic-driven oscillator in the rotating-wave approximation takes the form

$$H = \hbar\Delta a^\dagger a + \hbar\chi(a^\dagger a)^2 + \hbar f(t)(\Omega a^\dagger + \Omega^* a). \tag{1}$$

Note that the time-dependent coupling constant $\Omega f(t)$ is proportional to the amplitude of the driving field, which consists of Gaussian pulses with duration T separated by time intervals τ as follows:

$$f(t) = \sum e^{-(t-t_0-n\tau)^2/T^2}. \tag{2}$$

Here, $a^\dagger$,a are the oscillatory creation and annihilation operators, respectively, χ is the nonlinearity strength, and $\Delta = \omega_0 - \omega$ is the detuning between the mean frequency of the driving field and the frequency of the oscillator. For $f(t) = 1$, this Hamiltonian describes a nonlinear oscillator driven by a monochromatic force.

The evolution of the system of interest is governed by the following master equation for the reduced density matrix in the interaction picture:

$$\frac{d\rho}{dt} = -\frac{i}{\hbar}[H,\rho] + \sum_{i=1,2}\left(L_i\rho L_i^\dagger - \frac{1}{2}L_i^\dagger L_i\rho - \frac{1}{2}\rho L_i^\dagger L_i\right), \tag{3}$$

where $L_1 = \sqrt{(N+1)\gamma}a$ and $L_2 = \sqrt{N\gamma}a^\dagger$ are the Lindblad operators, γ is a dissipation rate, and N denotes the mean number of quanta of a heat bath. To study the pure quantum effects, we focus below on the case of very low reservoir temperature, which, however, ought to be still larger than the characteristic temperature $\mathcal{T} \gg \mathcal{T}_{cr} = \hbar\gamma/k_B$.

The Hamiltonian (1) describes a wide range of physical systems, including nanomechanical oscillator, Josephson junction device, optical fibers, quantum dots, and quantum scissors (we have noted a few of these systems in Sec. I). Note that quantum effects in a NDO with a time-modulated driving force including the pulsed regime have been studied in a series of papers [51–56].

Our numerical simulation of Eq. (3) is based on the method of quantum state diffusion (QSD) (see Ref. [57] and, for example, applications in Refs. [51–56] and [58–61]). For clarity, we choose the mean number of reservoir photons $N = 0$ in our numerical calculation. Note that for $N \ll 1$, this restriction is valid for the majority of problems in quantum optics and, in particular, for the schemes involving a nanomechanical oscillator and Josephson junction. In experiments, the nonlinear oscillator based on the current-biased JJ is cooled down to a temperature of $\mathcal{T} = 20$ mK, which corresponds to $N = 0.0013$, whereas $\mathcal{T}_{cr} = 10^{-5}$ K for $\gamma = 1$ MHz.

On the other hand, the corresponding equation of motion for the dimensionless amplitude of the oscillatory mode in the semiclassical approach has the following form:

$$\frac{d\alpha}{dt} = -i[\Delta + \chi + 2|\alpha|^2\chi]\alpha + if(t)\Omega - \gamma\alpha. \tag{4}$$

This equation modifies the standard Duffing equation in the case of the NDO with time-dependent coefficient. It will be useful for the comparison of results obtained from the quantum approach with the analogous ones in the semiclassical limit.

III. BISTABILITY AT LEVEL OF A FEW QUANTA

First, we describe the NDO driven by monochromatic force [i.e., $f(t) = 1$ in the Hamiltonian described by (1)] in the bistable regime. Based on the semiclassical approach given by Eq. (4), the bistable dynamics is realized if the following inequalities are satisfied [27]:

$$\begin{gathered}\chi(\Delta + \chi) < 0, \\ |(\Delta + \chi)/0.5\gamma| > \sqrt{3}, \\ \left[1 + \frac{27\chi\Omega^2}{(\Delta+\chi)^3} + \left(\frac{1.5\gamma}{\Delta+\chi}\right)^2\right]^2 < \left[1 - 3\left(\frac{\gamma/2}{\chi+\Delta}\right)^2\right]^3.\end{gathered} \tag{5}$$

With this range of parameters, the typical hysteresis curves depending on the detuning Δ and force amplitude Ω are displayed in the system [27]. The result for the stationary excitation number $n = |\alpha|^2$ can be obtained by solving the following equation:

$$|\alpha|^2 = \frac{\Omega^2}{(\Delta + \chi + 2\chi|\alpha|^2)^2 + \gamma^2}, \tag{6}$$

and is depicted in Fig. 1.

It is well known that whereas the semiclassical result exhibits hysteresis-cycle behavior, the corresponding quantum mechanical result, which accounts for the influence of quantum noise, shows a gradual evolution. This can be observed from the exact quantum solution for the mean excitation number in the following form:

$$\langle a^\dagger a\rangle = \frac{\Omega^2}{(\Delta+\chi)^2 + (\gamma/2)^2}\frac{F(c+1,c^*+1,z)}{F(c,c^*,z)}, \tag{7}$$

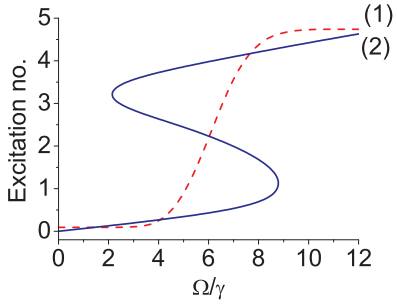

FIG. 1. (Color online) The mean excitation number of an anharmonic oscillator: (1) quantum solution and (2) semiclassical solution. The parameters are as follows: $\Delta/\gamma = -15$, $\chi/\gamma = 2$.

where $F = F_2$ is the generalized hypergeometric function, and c and z are coefficients that depend on the parameters, $c = (\Delta + \chi)/\chi - i\gamma/(2\chi)$ and $z = 2(\Omega/\chi)^2$.

It is also observed that the characteristic threshold behavior, which is determined by a drastic increase of the intensity in the transition region, disappears as the relative nonlinearity χ/γ increases. In Fig. 1, we have plotted both the semiclassical and quantum solutions corresponding to Eqs. (6) and (7).

More detailed information on the quantum-statistical properties of the oscillatory mode in the bistable range can be obtained from the analysis of the excitation number probability distribution function $p(n)$, but not from the mean excitation number. In this way, the locations of extrema of the $p(n)$ function, i.e., the locations of the most and least probable values of n, may be identified with the semiclassical stable and unstable steady states in the limit of small quantum noise level [62,63]. With the increase of χ/γ, the curve of locations of these extrema which depend on Ω becomes shifted from the corresponding semiclassical curve for the mean excitation number.

For this reason, we have analyzed quantum bistability in phase space in the framework of the Wigner function that gives the most complete description of quantum systems and can be measured by methods of quantum tomography. The analogous investigations of bistability have already been done in the area of single-atom cavity quantum electrodynamics. Therefore, bistable behavior on few photon regimes has been studied theoretically [40,41] and experimentally [42] on local maxima and minima curves as well as on the Q function in phase space by a comparison of the semiclassical and quantum treatments.

Considering bistability at low levels of quanta, it is natural to pose the following question: what is the minimal low level range of excitation numbers at which bistability is displayed in the strong quantum regime? Below, we shall discuss this problem based on quantum trajectories and the Wigner function for the case of quantum dynamics, and the Poincaré section for the case of semiclassical dynamics.

We shall use the numerical method, instead of the analytical results obtained in terms of the exact solution of the Fokker-Planck equation [63–65], to analyze the monochromatically driven NDO at low levels of quanta within the overtransient time intervals $t \gg \gamma^{-1}$. The reason is that the steady-state solution of the Fokker-Planck equation has been found using the standard approximation method of potential equations. Here, the validity of this solution is checked in the low levels of quanta that require a high nonlinearity with respect to dissipation.

We employ the Wigner function

$$W(r,\theta) = \sum_{n,m}\rho_{nm}(t)W_{mn}(r,\theta) \tag{8}$$

in terms of the matrix elements $\rho_{nm} = \langle n|\rho|m\rangle$ of the density matrix operator in the Fock state representation. Here, (r,θ) are the polar coordinates in the plane of complex phase space, $x = r\cos\theta$, $y = r\sin\theta$, while the coefficients $W_{mn}(r,\theta)$ are the Fourier transform of matrix elements of the Wigner characteristic function.

The properties of the bistable dynamics at the level of a few excitation number are illustrated in Fig. 2. Figure 2(a) shows

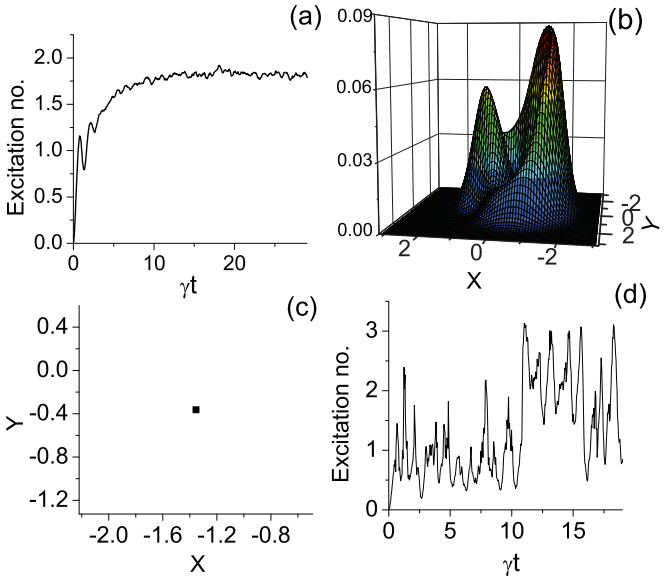

FIG. 2. (Color online) (a) The time evolution of the mean excitation numbers of the oscillatory mode, (b) the Wigner function, (c) the semiclassical Poincaré section, and (d) the time evolution of the excitation numbers along a single trajectory. The parameters are as follows: $\Delta/\gamma = -8$, $\chi/\gamma = 2$, and $\Omega/\gamma = 2.7$.

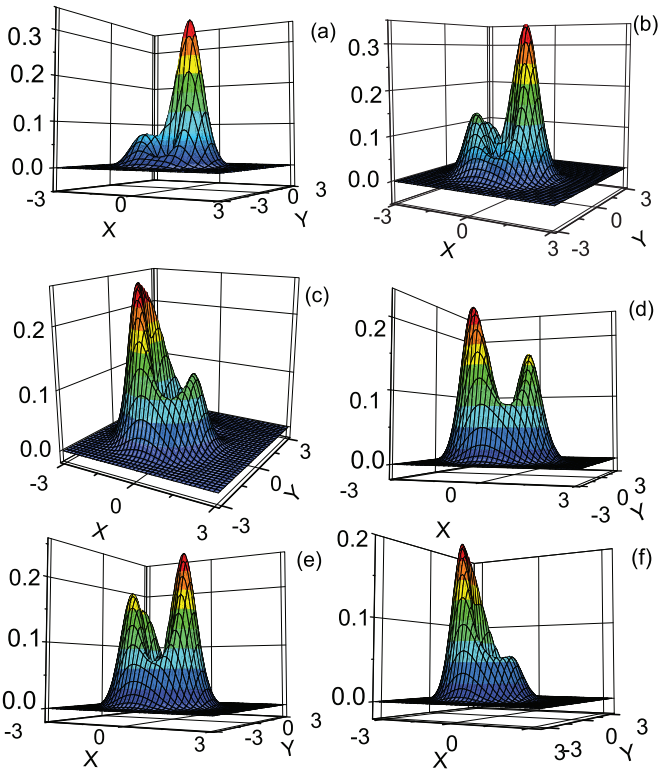

FIG. 3. (Color online) The Wigner functions for the oscillatory mode against the amplitude of the external force. The parameters are as follows: $\Delta/\gamma = -8$, $\chi/\gamma = 2$, and (a) $\Omega/\gamma = 2.1$, (b) $\Omega/\gamma = 2.3$, (c) $\Omega/\gamma = 2.5$, (d) $\Omega/\gamma = 2.7$, (e) $\Omega/\gamma = 2.9$, and (f) $\Omega/\gamma = 3.1$.

that the mean excitation number is small, which implies that the system is operating in the deep quantum regime. In Fig. 2(d), we have plotted one single quantum stochastic trajectory for excitation number by setting the system initially in the vacuum oscillatory state, and consider time dependence over a long time compared to the characteristic dissipative time. As expected, the analysis of the time-dependent stochastic trajectories after taking the expectation shows that the system spends most of its time close to one of the semiclassical bistable solutions with quantum interstate transitions occurring at random intervals.

In order to demonstrate the occurrence of bistability in phase space, we tune the parameters of the nonlinear oscillator to satisfy the set of inequalities given by Eq. (5). As our calculations show, the Wigner function displays two peaks [Fig. 2(b)] which indicate bistability. On the other hand, the Poincaré section, which is obtained from the semiclassical calculations of Eq. (4), shows a single point in phase space [Fig. 2(c)], corresponding to the presence of regular dynamics. Thus, for this set of parameters, we have distinctly demonstrated the difference between the semiclassical and quantum treatment of bistability in phase space for the low levels of quanta. In Sec. IV, we will present the other pure quantum effect in bistable behavior, which concerns the production of quantum superposition.

Further investigation of the model has allowed us to establish additional properties of dissipative bistable dynamics. For this purpose, we have shown in Fig. 3 the occurrence of bistability in phase space against the amplitude of the external force. We observe that for the given parameters of detuning and nonlinearity, there is an intermediate range of amplitudes where bistability takes place.

It is also interesting to consider the behavior of the NDO by using the scaling properties of Eq. (4). Indeed, it is easy to verify that this equation is invariant with respect to the following scaling transformation of the complex amplitude: $\alpha' \to \lambda\alpha, \chi' \to \chi/\lambda^2, \Omega' \to \lambda\Omega, \Delta' \to \Delta + \chi(1 - 1/\lambda^2)$. Thus, for $\lambda > 1$, oscillatory excitation numbers are increased via the scaling transformation. It is interesting to analyze such scaling from the point of view of quantum-statistical theory, and its relevance to decoherence and dissipation. By using the scaling properties, we can consider the system for various excitation numbers. The Wigner functions for the scaled $\lambda = 2$ and $\lambda = 3$ are presented in Fig. 4. As shown in the figure, increasing λ leads to a suppression of one of the peaks in the Wigner function and on the whole, the bistability of the system

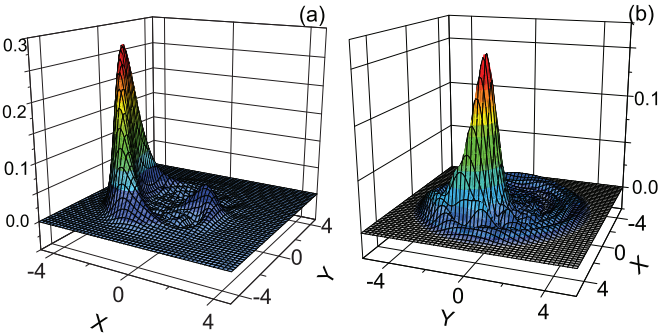

FIG. 4. (Color online) (a) The Wigner function for (a) $\lambda = 2$ and (b) $\lambda = 3$. The parameters are as follows: $\Delta/\gamma = -8$, $\chi/\gamma = 2$, and $\Omega/\gamma = 2.7$.

has vanished. Hence, we have shown that such parameter scaling does not arise in the low levels of quanta of the NDO.

There is a detection boundary of bistable states at the limit of small excitation numbers in phase space in accordance with the Planck uncertainty principle. By accounting for $\Delta X \Delta P \geqslant 1/2$, where X and P are dimensionless position and momentum operators and $n = |\alpha|^2$ with $\alpha = X + iP$, it seems that for a small enough level of excitation numbers, we cannot distinguish between the two branches of bistability. In this case, the size of the contour plots of the Wigner functions is sufficiently squeezed, such that the two bistable branches are too close with respect to each other to be distinguishable.

IV. QUANTUM INTERFERENCE ASSISTED BY BISTABILITY

In this section, we demonstrate that it is possible to create quantum superposition in bistable dynamics of the NDO under pulsed excitation. Indeed, the application of time-dependent force can lead to a transition between the two branches of the system dynamics in the bistable regime, and open an opportunity to generate interference between them. However, quantum interference takes place at a very short time interval and disappears due to dissipation and decoherence. In order to recover the quantum interference beyond the transient regimes, we suggest the application of a specific train of Gaussian pulses according to the model considered in Sec. II. The results depicted in Fig. 5 shows that with the applied Gaussian pulse, the Wigner function has negative ranges. The Wigner functions are found to possess two humps, which correspond to the bistable branches in phase space, and there is also the occurrence of an interference pattern between them.

In order to be sure that the effects of dissipation and decoherence in the oscillatory mode at transient time are suppressed when the train of pulses is applied, we proceed to calculate the purity of the state, i.e., $\mathrm{Tr}(\rho^2)$. Note that for a pure state, $\mathrm{Tr}(\rho^2) = 1$. The results for the dependence of $\mathrm{Tr}(\rho^2)$ on the pulse duration T and the time intervals between pulses τ are depicted in Fig. 6 for the overtransient regime, i.e., for time intervals $t \gg \gamma^{-1}$. In Fig. 6(a), which corresponds to a variation of pulse duration for a fixed τ of 2.5, we notice that the purity is maximal for very short pulses and decreases monotonically as T increases. The opposite behavior is observed, however, for the case when the time

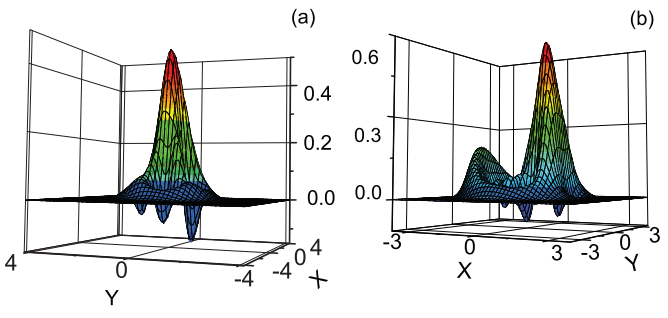

FIG. 5. (Color online) The Wigner functions showing quantum-interference patterns. The parameters are as follows: $\Delta/\gamma = -8$, $\chi/\gamma = 2$, $\Omega/\gamma = 2.7$, (a) $T = 0.5\gamma^{-1}$, $\tau = 2\gamma^{-1}$, and (b) $T = 0.1\gamma^{-1}$, $\tau = 2\gamma^{-1}$.

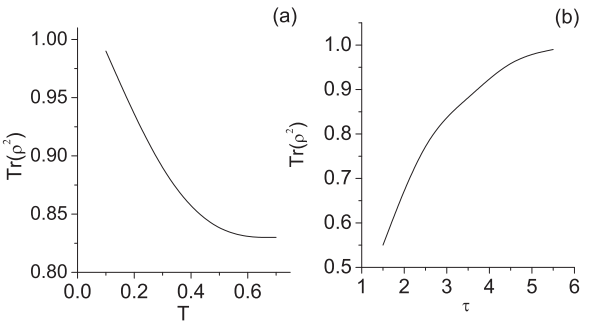

FIG. 6. The dependence of purity (a) on T for fixed $\tau = 2.5\gamma^{-1}$ and (b) on τ for fixed $T = 0.5\gamma^{-1}$. The rest of the parameters are $\Delta/\gamma = -8$, $\chi/\gamma = 2$, and $\Omega/\gamma = 2.7$.

interval between pulses is varied while the pulse duration is fixed, as displayed in Fig. 6(b).

V. QUANTUM DISSIPATIVE CHAOS AT LOW LEVELS OF EXCITATION NUMBERS

In this section, we demonstrate that dissipative chaos is realized in the strong quantum regime of NDO at low levels of quanta. The chaotic regime appears in the NDO when driven by a train of Gaussian pulses, and it depends on the duration T of the pulses and the time intervals τ between them.

Many criteria have been suggested to define chaos in quantum systems, varying in their emphasis and domain of application. Nevertheless, as yet, there is no universally accepted definition of quantum chaos. Our analysis is given in the framework of semiclassical and quantum distributions by using a correspondence between contour plots of the Wigner function and the Poincaré section. Such analysis has been proposed and realized [53] in the mesoscopic regimes of NDO with time-dependent coefficients.

It is well known that the Poincaré section has the form of strange attractor in phase space for dissipative chaotic systems, while it has the form of close contours with separatrices for Hamiltonian systems. Thus, in this paper, we demonstrate the quantum chaotic regime by means of a comparison between the contour plots of the Wigner functions and the strange attractors on the classical Poincaré section. In this way, we calculate the Wigner function in phase space by averaging an ensemble of quantum trajectories for definite time intervals. On the other hand, the Poincaré section is calculated through the semiclassical distribution based on Eq. (4), but for a large number of time intervals: it is constructed by fixing points in phase space at a sequence of periodic intervals. Note that such analysis seems to be rather qualitative than quantitative for the ranges of low level, oscillatory excitation numbers, where the validity of the semiclassical equation is questionable. Indeed, it is shown below that the semiclassical and quantum treatments of quantum dissipative chaos are cardinally different in the deep quantum regime.

The typical results of calculations are depicted below. Note that the ensemble-averaged mean oscillatory excitation number and the Wigner functions are nonstationary and exhibit a periodic time-dependent behavior, i.e., they repeat the periodicity of the driving pulses at the overtransient regime. In this nonstationary regime, the Poincaré section depends on

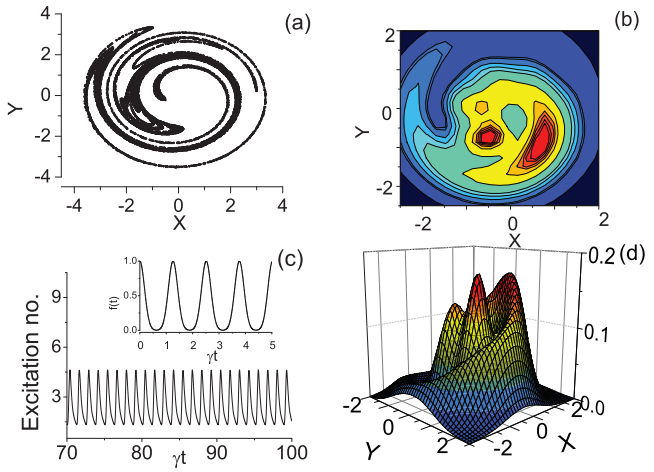

FIG. 7. (Color online) (a) The Poincaré section, (b) the contour plot of the Wigner function, (c) the excitation number time series with snapshots of Gaussian pulses as inset, and (d) the Wigner function. The parameters are as follows: $\chi/\gamma = 0.7, \Omega/\gamma = 20.4, \Delta/\gamma = -15$, $T = 0.25\gamma^{-1}, \tau = 2\pi/5\gamma$. Note that these distributions occur at time $\gamma t = 100$ with the mean excitation number of 1.54. The range of excitation numbers is 1.26 to 4.98.

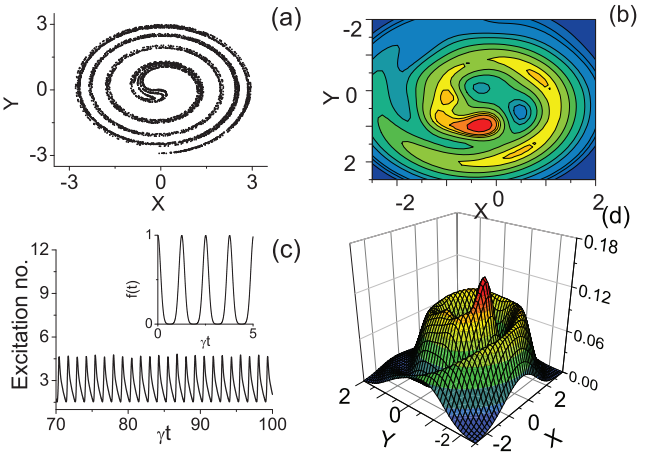

FIG. 9. (Color online) (a) The Poincaré section, (b) the contour plot of the Wigner function, (c) the excitation number time series with snapshots of Gaussian pulses as inset, and (d) the Wigner function. The parameters are $\chi/\gamma = 0.7, \Omega/\gamma = 20.4, \Delta/\gamma = -15$, $T = 0.15\gamma^{-1}, \tau = 2\pi/5\gamma$. Note that these distributions occur at time $\gamma t = 100$ with the mean excitation number of 2.04. The range of excitation numbers is 1.43 to 5.13.

the initial time interval t_0. We choose various initial times t_0 in order to ensure that they match with the corresponding time intervals of the Wigner function. In Figs. 7–10, we show the typical semiclassical and quantum distributions for the parameters Δ/γ, χ/γ, Ω/γ which correspond to the chaotic regimes, and for various durations of the Gaussian pulses. In the following, we shall study the quantum phase space dynamics that have a chaotic classical counterpart.

It is observed that the figures of Poincaré sections clearly indicate a classical strange attractor with fractal structure that is typical of chaotic dynamics. The Wigner functions have spiral (helical) structures (Figs. 7–10) that reflect a chaotic regime in analogy to the corresponding Poincaré sections, and their contour plots are concentrated approximately around the attractor. It is important to note that such qualitative correspondence is only used to demonstrate a chaotic regime in quantum treatment based on the Wigner function. However, the Wigner function, being a quantum quasiprobability distribution, also describes the quantum effects. Hence, in the deep quantum regime, the different branches of the attractors are hardly resolved in the Wigner functions that show the delocalization due to quantum noise. Among these pure quantum effects, we especially note the occurrence of superposition states and quantum interference effects that

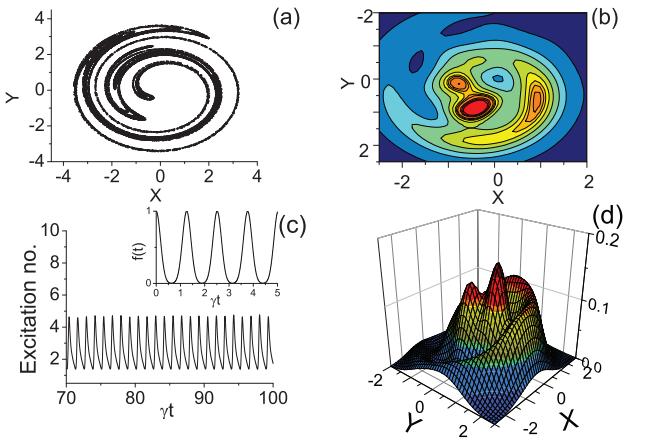

FIG. 8. (Color online) (a) The Poincaré section, (b) the contour plot of the Wigner function, (c) the excitation number time series with snapshots of Gaussian pulses as inset, and (d) the Wigner function. The parameters are $\chi/\gamma = 0.7, \Omega/\gamma = 20.4, \Delta/\gamma = -15$, $T = 0.205\gamma^{-1}$, $\tau = 2\pi/5\gamma$. Note that these distributions occur at time $\gamma t = 100$ with the mean excitation number of 1.74. The range of excitation numbers is 1.29 to 5.11.

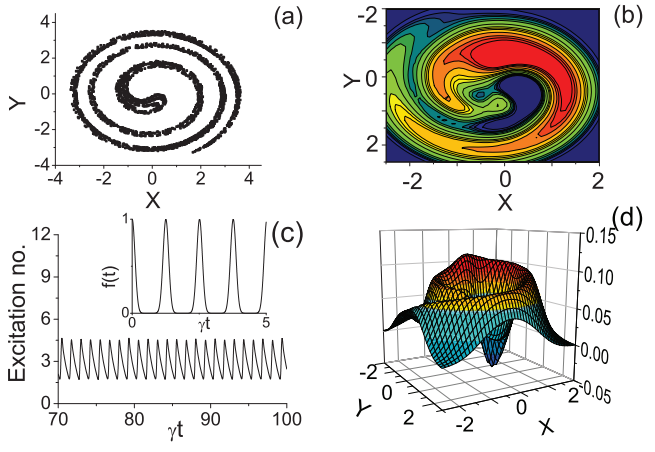

FIG. 10. (Color online) (a) The Poincaré section, (b) the contour plot of the Wigner function, (c) the excitation number time series with snapshots of Gaussian pulses as inset, and (d) the Wigner function. The parameters are $\chi/\gamma = 0.7, \Omega/\gamma = 20.4, \Delta/\gamma = -15$, $T = 0.1\gamma^{-1}, \tau = 2\pi/5\gamma$. Note that these distributions occur at time $\gamma t = 100$ with the mean excitation number of 2.46. The range of excitation numbers is 1.62 to 4.83.

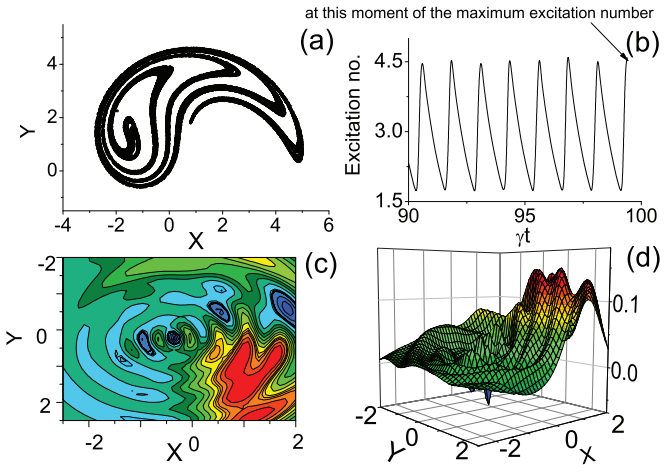

FIG. 11. (Color online) (a) The Poincaré section, (b) the excitation number time series, (c) the contour plot of the Wigner function, and (d) the Wigner function at the moment $\gamma t = 100.6$ when the excitation number is maximum. The parameters are $\chi/\gamma = 0.7$, $\Omega/\gamma = 20.4$, $\Delta/\gamma = -15$, $T = 0.1\gamma^{-1}$, $\tau = 2\pi/5\gamma$.

assist the chaotic behavior in the low levels of quanta. Indeed, it should be specified that the Wigner function for the regime presented in Fig. 10 has a region of negative values. These effects, which correspond to quantum interference in phase space, vanish in the semiclassical approach. The demonstration of these and other quantum effects for both dissipative bistable and chaotic dynamics is one of the remarkable results of this paper.

The chaotic dynamics of the oscillatory mode strongly depends on the time interval t. To demonstrate this point, in Figs. 11 and 12, we depict the Wigner function and the Poincaré section for the oscillatory parameters used in Fig. 10, but for the other time intervals of t within the duration of pulses which correspond to the maximal and minimal values of the number of excitation number.

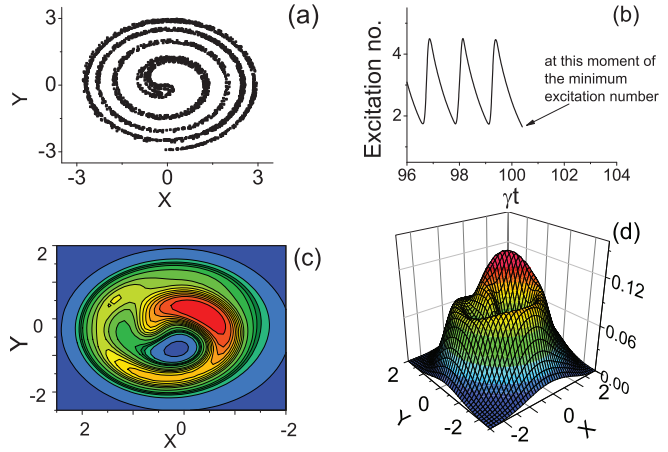

FIG. 12. (Color online) (a) The Poincaré section, (b) the excitation number time series, (c) the contour plot of the Wigner function, and (d) the Wigner function at the moment $\gamma t = 100.4$ when the excitation number is minimum. The parameters are as follows: $\chi/\gamma = 0.7$, $\Omega/\gamma = 20.4$, $\Delta/\gamma = -15$, $T = 0.1\gamma^{-1}$, $\tau = 2\pi/5\gamma$.

At the end of this section, we explore the transition from regular to chaotic regimes that is realized through varying the strength of the pulse trains by considering cases of small excitation numbers. We note that the studies of transition to chaos have a long history. Nevertheless, important outstanding questions related to quantum-classical correspondence have been raised recently, such as the question of how to recover classical (chaotic) dynamics in open quantum systems subject to decoherence (see, for example, [47]). Here we have employed an experimentally available model which is a modification of a very popular system-kicked oscillator model with driving by Gaussian pulses. It is thus natural for us to include a discussion of various regimes of this oscillator, which encompasses also the regime of transition to quantum chaos for completeness.

For this goal, we first present our results on semiclassical approximation based on an analysis of the Lyapunov exponents of the semiclassical time series [66]. This quantity is determined as $L = \frac{1}{\Delta t} \ln \frac{\|x_2(t) - x_1(t)\|}{\|x_2(t_0) - x_1(t_0)\|}$; here, $x = [\mathrm{Re}(\alpha), \mathrm{Im}(\alpha), \beta]$, where β is the time variable defined through $d\beta/dt = 1$ which augments Eq. (4) to create an autonomous system. Note that x_2 and x_1 represent two trajectories that are very close together at the initial time t_0. Furthermore, $\Delta t = t - t_0$, with $t \to \infty$. For $L > 0$, the system shows chaotic dynamics. $L = 0$ corresponds to the case of conservative regular systems, and $L < 0$ indicates that the dissipative system is regular. We examine the exponents for time intervals corresponding to the minimal and maximal excitation numbers of the oscillatory mode with dependence from the parameter Ω/γ. The results are depicted in Figs. 13 and 14 for the constant parameters: Δ/γ and χ/γ. We observe a transition from regular to chaotic behavior at $\Omega/\gamma = 12.55$ for minimal and maximal excitation number of the oscillatory mode. Note that this transition occurs at the low oscillatory number from the minimum $n = 0.94$ to the maximum $n = 2.70$. Thus, when the strength of the pulse trains Ω/γ is low, we observe regular behavior; and as a critical threshold is crossed, the system behaves chaotically. Interestingly, a closer scrutiny of the dynamics of the system reveals a regime of transient chaos in the

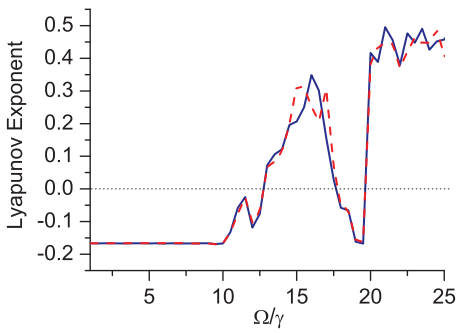

FIG. 13. (Color online) The largest Lyapunov exponent of the semiclassical dynamics vs the strength of the pulse trains. The solid (blue) curve corresponds to the moment of maximum excitation number at $\gamma t = 39.1$ for $1 \leqslant \Omega/\gamma \leqslant 19$ and at $\gamma t = 39$ for $19.5 \leqslant \Omega/\gamma \leqslant 26$. The dashed (red) curve corresponds to the moment of minimum excitation number at $\gamma t = 40.2$ for $1 \leqslant \Omega/\gamma \leqslant 8.5$ and at $\gamma t = 40.1$ for $9 \leqslant \Omega/\gamma \leqslant 26$. The rest of the parameters are $\chi/\gamma = 0.7$, $\Delta/\gamma = -15$, $T = 0.1\gamma^{-1}$, $\tau = 2\pi/5\gamma$.

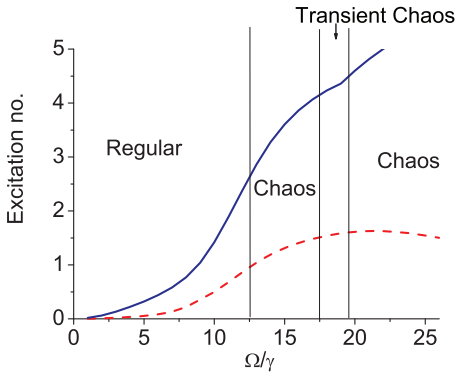

FIG. 14. (Color online) The plot of the maximum and minimum excitation number vs the strength of the pulse trains that correspond to the case of Fig. 13. The solid (blue) curve is for the maximum excitation number and the dashed (red) curve is for the minimum excitation number. Note that the regular, transient chaos, and chaos regimes of the corresponding semiclassical dynamics are also indicated in the plot.

range $17.61 \leqslant \Omega/\gamma \leqslant 19.56$, whereupon the semiclassical dynamics rattle about chaotically for some time before settling down to regular behavior which leads to a window of negative Lyapunov exponents. Then, beyond $\Omega/\gamma = 19.56$, chaotic attractors are found to emerge again in the Poincaré section. It is important to note that analogous dynamical behavior is observed to arise at both the moments when the excitation number is a minimum and a maximum (see Fig. 13).

In summary, we have uncovered the parameters for which a decrease of the excitation number leads to a transition of the system from a chaotic to regular regime in the classical treatment. Another situation is realized in the quantum treatment. Indeed, for these regimes of low excitation, quantum noise and quantum effects play an essential role in the formation of the oscillatory dynamics, and in particular, in the realization of chaotic dynamics and scenarios of transition from a chaotic to regular regime. This statement is also confirmed by the calculation of the Wigner function. We observe that below the transition threshold of $\Omega/\gamma = 12.55$, the Wigner function has the form of a single hump. Beyond the transition threshold, the hump starts to spread and a spiral begins to form. These changes are found to happen continuously and smoothly in the Wigner function as Ω/γ increases. However, as Ω/γ goes above 19.56, the Wigner functions are observed to quickly take the appearance of a strange attractor. Our results here thus clearly show the presence of good quantum-classical correspondence in the quantum and classical dynamical behavior. In addition, our results also demonstrate that quantum NDO, which is a form of quantum anharmonic oscillators, possess a rich set of dynamical behavior and properties that may be potentially useful for many practical purposes [67,68].

VI. SUMMARY

To summarize, we have studied the problem of quantum chaos and bistability at the level of few excitation numbers of NDO that is interacting with an external field and a background environment leading to dissipation and decoherence. We have analyzed the formation of bistable behavior and chaotic regime of NDO at the low oscillatory excitation numbers when the ratio χ/γ is chosen from 0.7 to 2. We perform a systematic numerical analysis based on numerical simulation of the master equation by using a quantum state diffusion method of quantum trajectories, where we have varied a number of relevant oscillatory parameters, Ω/γ, Δ/γ, and the parameters of Gaussian pulses. Thus, the combination of results gives a rather thorough understanding of the NDO in the low levels of quanta, as well as a simple picture of the formation of bistability and chaos at low levels of quanta in phase space. We have also found unexpected features of NDO in phase space. It has been demonstrated that the Wigner functions of the oscillatory mode in both bistable and chaotic regimes realized due to interaction with a train of Gaussian pulses acquire negative values and interference patterns in certain parts of phase space. We have demonstrated that in the case of bistable dynamics, the Wigner functions describe two humps corresponding to the bistable branches and interference pattern between them in phase space, while for the chaotic regime, the Wigner functions have spiral structures (which correspond to a strange attractor in Poincaré sections) with a deep well, showing negativity of the Wigner function [Fig. 10(d)]. Quantum interference in phase space is realized in the overtransient regime by driving the oscillator via a series of short pulses with proper parameters for the effective reduction of dissipative and decoherence effects. Our results can be tested with available experimental systems as noted in Sec. I.

[1] J. Q. You and F. Nori, Nature (London) **474**, 585 (2011).
[2] Iulia Buluta, Sahel Ashhab, and Franco Nori, Rep. Prog. Phys. **74**, 104401 (2011).
[3] Y. Makhlin, G. Schön, and A. Shnirman, Rev. Mod. Phys. **73**, 357 (2001).
[4] D. I. Schuster *et al.*, Nature (London) **445**, 515 (2007).
[5] A. Fragner *et al.*, Science **322**, 1357 (2008).
[6] O. Astafiev *et al.*, Nature (London) **449**, 588 (2007).
[7] M. Neeley *et al.*, Science **325**, 722 (2009).
[8] O. Astafiev *et al.*, Science **327**, 840 (2010).
[9] E. Hoskinson, F. Lecocq, N. Didier, A. Fay, F. W. J. Hekking, W. Guichard, O. Buisson, R. Dolata, B. Mackrodt, and A. B. Zorin, Phys. Rev. Lett. **102**, 097004 (2009).
[10] J. Claudon, A. Zazunov, F. W. J. Hekking, and O. Buisson, Phys. Rev. B **78**, 184503 (2008).
[11] H. G. Craighead, Science **290**, 1532 (2000).
[12] M. L. Roukes, Phys. World, **14**, 25 (2001).
[13] A. N. Cleland, *Foundations of Nanomechanics* (Springer, Berlin, 2003).
[14] K. L. Ekinci and M. L. Roukes, Rev. Sci. Instrum. **76**, 061101 (2005).
[15] K. Jensen, K. Kwanpyo, and A. Zettl, Nat. Nanotech. **3**, 533 (2008).
[16] A. Cleland, and M. Roukes, Nature (London) **392**, 160 (1998).
[17] D. Rugar, R. Budakian, H. Mamin, and B. Chui, Nature (London) **430**, 329 (2004).

[18] Keith C. Schwab, E. A. Henriksen, J. M. Worlock, and Michael L. Roukes, Nature (London) **404**, 974 (2000).
[19] Miles P. Blencowe, Phys. Rep. **395**, 159 (2004).
[20] I. Wilson-Rae, N. Nooshi, W. Zwerger, and T. J. Kippenberg, Phys. Rev. Lett. **99**, 093901 (2007).
[21] F. Marquardt, J. P. Chen, A. A. Clerk, and S. M. Girvin, Phys. Rev. Lett. **99**, 093902 (2007).
[22] T. Rocheleau, T. Ndukum, C. Macklin, J. B. Hertzberg, A. A. Clerk, and K. C. Schwab, Nature (London) **463**, 72 (2010).
[23] A. D. O'Connell *et al*., Nature (London) **464**, 697 (2010).
[24] J. D. Teufel, T. Donner, Li Dale, J. H. Harlow, M. S. Allman, K. Cicak, A. J. Sirois, J. D. Whittaker, K. W. Lehnert, and R. W. Simmonds, Nature (London) **475**, 35 (2011).
[25] J. Chan, T. P. Mayer Alegre, A. H. Safavi-Naeini, J. T. Hill, A. Krause, S. Gröblacher, M. Aspelmeyer, and O. Painter, Nature (London) **478**, 89 (2011).
[26] X. Wang, S. Vinjanampathy, F. W. Strauch, and K. Jacobs, Phys. Rev. Lett. **107**, 177204 (2011).
[27] P. D. Drummond and D. F. Walls, J. Phys. A: Math. Gen. **13**, 725 (1980).
[28] R. Vijay, M. H. Devoret, and I. Siddiqi, Rev. Sci. Instrum. **80**, 111101 (2009).
[29] I. Siddiqi, R. Vijay, F. Pierre, C. M. Wilson, M. Metcalfe, C. Rigetti, L. Frunzio, and M. H. Devoret, Phys. Rev. Lett. **93**, 207002 (2004).
[30] I. Siddiqi, R. Vijay, F. Pierre, C. M. Wilson, L. Frunzio, M. Metcalfe, C. Rigetti, R. J. Schoelkopf, M. H. Devoret, D. Vion, and D. Esteve, Phys. Rev. Lett. **94**, 027005 (2005).
[31] I. Katz, A. Retzker, R. Straub, and R. Lifshitz, Phys. Rev. Lett. **99**, 040404 (2007).
[32] V. Peano and M. Thorwart, Chem. Phys. **322**, 135 (2006).
[33] M. Marthaler and M. I. Dykman, Phys. Rev. A **73**, 042108 (2006).
[34] M. I. Dykman, Phys. Rev. E **75**, 011101 (2007).
[35] C. K. Law and J. H. Eberly, Phys. Rev. Lett. **76**, 1055 (1996).
[36] D. M. Meekhof, C. Monroe, B. E. King, W. M. Itano, and D. J. Wineland, Phys. Rev. Lett. **76**, 1796 (1996).
[37] B. T. H. Varcoe *et al*., Nature (London) **403**, 743 (2000); P. Bertet, S. Osnaghi, P. Milman, A. Auffeves, P. Maioli, M. Brune, J. M. Raimond, and S. Haroche, Phys. Rev. Lett. **88**, 143601 (2002); E. Waks, E. Dimanti, and Y. Yamamoto, New J. Phys. **8**, 4 (2006).
[38] M. Hofheinz *et al*., Nature (London) **454**, 310 (2008); **459**, 546 (2009).
[39] T. V. Gevorgyan, A. R. Shahinyan, and G. Yu. Kryuchkyan, Phys. Rev. A **85**, 053802 (2012).
[40] C. M. Savage and H. J. Carmichael, IEEE J. Quantum Electron. **24**, 1495 (1988).
[41] M. A. Armen and H. Mabuchi, Phys. Rev. A **73**, 063801 (2006).
[42] J. Kerckhoff, M. A. Armen, and H. Mabuchi, Opt. Express **19**, 24482 (2011).
[43] H. Ammann, R. Gray, I. Shvarchuck, and N. Christensen, Phys. Rev. Lett. **80**, 4111 (1998).
[44] B. G. Klappauf, W. H. Oskay, D. A. Steck, and M. G. Raizen, Phys. Rev. Lett. **81**, 1203 (1998); **82**, 241 (1999).
[45] G. J. Milburn and C. A. Holmes, Phys. Rev. A **44**, 4704 (1991).
[46] J. K. Breslin, C. A. Holmes, and G. J. Milburn, Phys. Rev. A **56**, 3022 (1997); A. J. Scott, C. A. Holmes, and G. J. Milburn, *ibid.* **61**, 013401 (1999).
[47] S. Chaudhury, A. Smith, B. E. Anderson, S. Ghose, and P. S. Jessen, Nature (London) **461**, 768 (2009).
[48] S. Ghose, P. Alsing, I. Deutsch, T. Bhattacharya, S. Habib, and K. Jacobs, Phys. Rev. A **67**, 052102 (2003); S. Ghose, P. Alsing, I. Deutsch, T. Bhattacharya, and S. Habib, *ibid.* **69**, 052116 (2004).
[49] W. Léonski and A. Kowalewska-Kudleszuk, Prog. Opt. **56**, 131 (2011); A. Miranowicz and W. Léonski, J. Opt. B: Quantum Semiclass. Opt. **6**, 943 (2004).
[50] M. A. Macovei, Phys. Rev. A **82**, 063815 (2010).
[51] T. V. Gevorgyan, A. R. Shahinyan, and G. Yu. Kryuchkyan, Phys. Rev. A **79**, 053828 (2009).
[52] H. H. Adamyan, S. B. Manvelyan, and G. Yu. Kryuchkyan, Phys. Rev. A **63**, 022102 (2001).
[53] H. H. Adamyan, S. B. Manvelyan, and G. Yu. Kryuchkyan, Phys. Rev. E **64**, 046219 (2001).
[54] G. Yu. Kryuchkyan and S. B. Manvelyan, Phys. Rev. Lett. **88**, 094101 (2002).
[55] G. Yu. Kryuchkyan and S. B. Manvelyan, Phys. Rev. A **68**, 013823 (2003).
[56] T. V. Gevorgyan, S. B. Manvelyan, A. R. Shahinyan, and G. Yu. Kryuchkyan, in *Modern Optics and Photonics: Atoms and Structured Media*, edited by G. Kryuchkyan, G. Gurzadyan, and A. Papoyan (World Scientific, Singapore, 2010).
[57] I. C. Percival, *Quantum State Diffusion* (Cambridge University Press, Cambridge, 2000).
[58] S. T. Gevorkyan, G. Yu. Kryuchkyan, and N. T. Muradyan, Phys. Rev. A **61**, 043805 (2000).
[59] G. Yu. Kryuchkyan and N. T. Muradyan, Phys. Lett. A **286**, 113 (2001).
[60] H. H. Adamyan and G. Yu. Kryuchkyan, Phys. Rev. A **74**, 023810 (2006).
[61] N. H. Adamyan, H. H. Adamyan, and G. Yu. Kryuchkyan, Phys. Rev. A **77**, 023820 (2008).
[62] L. A. Lugiato, in *Progress in Optics*, edited by E. Wolf, Vol. XXI (North-Holland, Amsterdam, 1984).
[63] G. Yu. Kryuchkyan and K. V. Kheruntsyan, Opt. Comm. **120**, 132 (1996).
[64] K. V. Kheruntsyan *et al*., Opt. Comm. **139**, 157 (1997).
[65] K. V. Kherunstyan, J. Opt. B: Quantum Semiclass. Opt. **1**, 225 (1999).
[66] J. C. Sprott, *Chaos and Time-Series Analysis* (Oxford University Press, Oxford, 2003).
[67] N. N. Chung and L. Y. Chew, Phys. Rev. E **80**, 016204 (2009).
[68] N. N. Chung and L. Y. Chew, Phys. Rev. A **80**, 012103 (2009).